RSC Sustainability

ROYAL SOCIETY OF CHEMISTRY

PAPER

View Article Online
View Journal



Cite this: DOI: 10.1039/d6su00113k

# Sustainable air plasma regeneration of screen-printed gold electrodes with enhanced electroactive surface area and biosensing performance

Sina Ardalan,*[a] Clara T. H. Tran,[b] Stuart T. Fraser,[bc] Marcela M. M. Bilek[bd] and Anna Ignaszak*[ae]

Miniaturized electroanalytical devices paired with screen-printed electrodes (SPE) are gaining popularity due to their compact design and minimal analyte requirements. However, their single-use nature and non-degradable polymer substrates with printed precious metals like gold limit their sustainability as biosensing interfaces. Disposing of each electrode after a single use is neither cost-effective nor sustainable. Herein, a green air plasma cleaning technique is introduced to regenerate multiple gold SPEs simultaneously within 10 minutes. Air plasma treatment resulted in surface hydrophilicity, significant reduction in surface nitrogen analyzed by X-ray photoelectron spectroscopy, and near-zero charge transfer resistance with a simplified equivalent circuit only limiting charge transfer processes by redox mass diffusion characterized by Warburg impedance. The regenerated electrode was reused to fabricate an electrochemical impedance spectroscopy-based biosensor using a thiol-modified thrombin-binding aptamer. A 1.24-fold increase in the electroactive surface area led to a 2-fold increase in thiol-modified ssDNA aptamer immobilization towards 50 nM thrombin with a 3-fold increase in the sensor signal. Air plasma cleaning is a sustainable and facile technique to regenerate contaminated gold SPEs for biosensor fabrication with enhanced capture probe loading and biosensing sensitivity.

Received 23rd February 2026
Accepted 28th May 2026

DOI: 10.1039/d6su00113k

rsc.li/rscsus



### Sustainability spotlight

The high demand for screen-printed electrodes (SPE) to fabricate electrochemical sensors, given their one-time use-only nature, poses environmental burdens and rapid consumption. Effective regeneration and recycling of SPEs are practices to move towards sustainable chemical processes for sensor/biosensor fabrication via green chemistry methods. Our developed rapid air plasma cleaning method recycles the disposed SPEs, regenerates their electrochemical activity, and enhances their sensitivity. The developed air plasma cleaning technique contributes to sustainable electrochemical sensor fabrication by green chemistry approaches (electrode waste prevention, re-engineering electrochemical sensors, less hazardous chemical treatment by using a dry/solventless plasma treatment, designing safer chemical treatment processes, regeneration instead of environmental depletion, and a safer surface treatment process). This report contributes to the UN sustainable development goals of industry, innovation, and infrastructure (SDG-9) and responsible consumption and production (SDG-12).

## Introduction

As an integral part of biomedical diagnostics, biosensors have become integral tools for healthcare professionals to detect biomolecules, disease-related biomarkers, pathogens, and viral infections. They are readily deployed, not only in a clinical setting, such as diagnostic laboratories, but also at the point-of-care, where they can be self-administered by non-professionals, as seen in continuous glucose monitoring devices.[1] Screen-printed electrodes (SPEs) have emerged as cost-effective substrates for electrochemical biosensors, that are particularly useful in healthcare and environmental monitoring.[2,3] SPEs are fabricated with industrial printers that deposit several layers and inks onto a flat base. This method supports large-scale production of affordable and sensitive sensors.[4] The SPE market is projected to expand at a Compound Annual Growth Rate (CAGR) of approximately 8.5% over the forecast period, with the market size reaching USD 500 million in 2024 and expected to grow to USD 898 million by 2033.[5]

Among these innovations, screen-printed gold electrodes (gold SPEs) are in high demand for developing electrochemical

[a]Department of Chemistry, University of New Brunswick, Fredericton, Canada. E-mail: sina.ardalan@unb.ca
[b]School of Biomedical Engineering, The University of Sydney, J03, NSW 2008, Australia
[c]Culturon Pty Ltd, Newtown, 2042, NSW, Australia
[d]School of Physics, The University of Sydney, A28, NSW 2006, Australia
[e]Department of Chemistry, Brock University, St. Catharines, Canada. E-mail: aignaszak@brocku.ca

biosensors.[6] Notably, many companies are manufacturing diverse types of gold SPEs, making the market highly competitive. Screen-printed biosensors are now being used for a wide range of applications such as clinical pathogen detection, biomarker discovery, environmental monitoring, pharmaceuticals, and the agro-food industry.[7]

Screen-printed gold electrodes (gold SPEs) are in high demand for developing electrochemical biosensors.[6] Gold SPEs provide a miniaturized platform that requires a minimal volume of analyte for the fabrication of electrochemical biosensors.[8] Despite the considerable advantages of gold SPEs for sensor fabrication, their major drawback is their lack of reusability.[9] This limitation is a result of surface saturation caused by bioreceptor immobilization and analyte binding, which hinders multiple uses and continuous analysis. The rigorous experimental trials involved in biosensor development require substantial quantities of gold SPEs which are typically designed for single-use and disposed of after testing. For instance, gold SPEs are commonly used for biosensor fabrication by forming covalent bonds with biologically active materials and bioreceptors through Au–S bonding.[10–14] To reuse the gold electrode, the entire biosensor interface must be completely removed to maintain its original electrochemical performance. This results in high consumption rates especially when optimizing conditions or dealing with experimental errors such as contamination during handling and storage.

Disposal of used gold SPEs and purchasing new ones presents economic and environmental challenges including precious metal waste. Gold's price has risen from US$1068 per troy ounce in December 2015 to a peak of US$2690 per troy ounce in December 2024.[15] Gold SPEs cost significantly more than carbon-based electrodes and are priced between 6.4 and 8.2 USD per electrode with a short lifespan. Considering the destructive impact of gold mining[16] and the recent surge in gold prices, it is important to explore methods for regenerating gold SPEs.

Gold electrodes can be recycled by chemical and electrochemical methods. However, these methods use toxic chemicals and processes. Previous research has primarily focused on pre-treating SPEs using electrochemical techniques, with a few studies investigating chemical and physical pre-treatment methods, such as plasma treatment.[17] For instance, argon plasma has shown to be an effective surface activation technique for carbon SPEs, *via* an etching process of polymer binder from the electrode surface exposing more carbon particles to the electrolyte solution.[18]

Plasma has numerous applications in surface treatment, thin film deposition, and sterilization.[19] One common surface treatment process is plasma cleaning that effectively removes organic contaminants, dust, grease, and other particulate matter. This method is highly efficient, non-contact (minimizing the risk of physical damage), eco-friendly (due to the absence of chemical solvents), and quick.[19] Air plasma cleaning is compatible with various electrode structures such as micro and nanoelectronics for non-destructive cleaning, as demonstrated by atomic force microscopy (AFM) and electrochemical measurements.[20] Alkane thiolate groups such as hexadecanethiolate SAMs, can be effectively detached by $H_2$ plasma in less than a minute, reducing the layer thickness from 22 Å to close to zero.[21] Additionally, $O_2$ plasma followed by ethanol reduction can fully regenerate the photolithographic gold layer from a gold oxide layer.[22] Argon plasma has shown to be an effective surface activation technique for carbon SPEs, *via* an etching process of polymer binder from the electrode surface exposing more carbon particles to the electrolyte solution.[18] Recently, innovative and rapid plasma treatment methods has been utilized to activate carbon and gold SPEs by a robotic plasma system.[23,24] This plasma system has shown to reduced charge-transfer resistance, increase electron-transfer kinetics and increased electroactive. However, it is unclear if the same activation/pretreatment procedure could be utilized in electrode recycling and detaching immobilized biomolecules.

Herein, we studied an air plasma cleaning technique to recover gold SPEs. The air plasma cleaning technique contributes to sustainable electrochemical sensor recycling by green chemistry approaches (electrode waste prevention, re-engineering electrochemical sensors, less hazardous chemical treatment by using a dry/solventless plasma treatment, designing safer chemical treatment processes, regeneration instead of environmental depletion, and a safer surface treatment process). The objective of this study is to develop an air plasma cleaning protocol to regenerate the gold SPEs that had been used for binding analysis of a model target protein, thrombin, to compliment the previous work that has been done on electrode activation and to extend the application of plasma treatment by sustainable plasma recycling in electrochemical biosensors. The used gold SPEs are referred to as electrodes on which a thiol-modified ssDNA aptamer was immobilized through SAM formation using thiol–gold chemisorption chemistry. They were then exposed to a thrombin solution for impedance-based binding analysis. Thrombin specifically binds to the aptamer through a high-affinity interaction (dissociation constant of $K_d \approx 5$ nM).[25] After the aptasensor is used for thrombin detection, it became coated with the covalently attached aptamer and the bound thrombin target. We used an air plasma cleaning technique to effectively regenerate gold SPEs by removing the surface bound ssDNA and thrombin. The effectiveness of plasma cleaning was assessed using electrochemical impedance spectroscopy (EIS), X-ray photoelectron spectroscopy (XPS), and contact angle (CA) measurements.

## Experimental section

### Materials

Potassium hexacyanoferrate(II) trihydrate ($Fe(CN)_6^{4-}$; 98.5%), potassium hexacyanoferrate(III) ($Fe(CN)_6^{3-}$; 99%), ethylenediaminetetraacetic acid (EDTA; 98.5%), tris(hydroxymethyl) aminomethane hydrochloride (Tris·HCl; >99%), mercaptohexanol (MCH; 99%) potassium chloride (KCl; 99%), sulfuric acid ($H_2SO_4$; 96%, p.a.), sodium hydroxide (NaOH; 98%, pellets), custom DNA oligo (aptamer; HPLC purified, 100 μM in TE buffer), and thrombin from human plasma (250 units, lyophilized powder, ≥2000 NIH units per mg) were purchased from Sigma-Aldrich. ItalSens gold Screen-Printed Electrode (gold

SPE; ∅ 3 mm working electrode) with printed silver pseudo reference electrode and a gold counter electrode was purchased from Palmsens (Netherlands).

All solutions were prepared with Milli-Q water. Except for protein and aptamer solutions, which were purchased in purified, DNase/RNase and protease-free form, all solutions were filtered using vacuum-driven filters (Stericup Quick Release, Sigma-Aldrich).

Aptamer and protein solutions were stored in low-binding tubes to reduce stickiness to the walls of the microtubes (DNA/Protein LoBind Tubes, Eppendorf). Low-retention pipette tips (ART, Thermo Fisher Scientific) were used for pipetting to minimize DNA/protein binding to pipette tips. All solutions, except $Fe(CN)_6^{3-}$, $Fe(CN)_6^{4-}$, $H_2SO_4$, protein, and aptamer solutions, were sterilized by autoclaving at 121 °C for 30 minutes, with a total cycle time of 1 hour.

A 10× stock solution of Tris-Buffered Saline (TBS) buffer was prepared by dissolving Tris·HCl and NaCl, then adjusting the pH to 7.4 with NaOH, with a final concentration of 200 mM Tris and 1500 mM NaCl. An electrochemical measurement buffer was prepared by mixing as-prepared TBS, $Mg^{2+}$ and $Fe(CN)_6^{3-/4-}$ stock solutions with the final concentrations of 1× TBS, 1 mM $Mg^{2+}$, and 1 mM $Fe(CN)_6^{3-/4-}$. An incubation buffer was prepared by mixing as-prepared TBS and $Mg^{2+}$ stock solutions with the final concentrations of 1× TBS and 1 mM $Mg^{2+}$. A 100 mM MCH stock solution was prepared by diluting MCH in water.

**Aptamer solution.** A 29-nucleotide single-stranded DNA aptamer against thrombin was chosen from the original research by Tasset *et al.*[26] HPLC-purified lyophilized aptamer was purchased from Sigma-Aldrich with the sequence of 5′-AGTCCGTGGTAGGGCAGGTTGGGGTGACT-3′ and a C6 S–S thiol-modifier on the 5′ end. Aliquots of a 5 μM aptamer solution were prepared in LoBind DNA microtubes diluted with TE buffer 1× and stored at 4 °C.

**Protein solution.** Thrombin (250 units) was purchased from Sigma-Aldrich (>2000 units per mg). Each unit corresponds to 0.324 μg, totalling 81 μg of thrombin. The molecular weight ($M_w$) of thrombin is 37.4 kDa. To calculate protein concentration, the equation $\mu M = (\mu g\ mL^{-1})/M_w$ in kDa was used.[27] The glass vial containing thrombin was first centrifuged at 4 °C at 3000 rpm to ensure complete settling of the thrombin. The thrombin-containing vial was then transferred to an ice bath, and thrombin was dissolved in cold Milli-Q water to a final concentration of 50 nM. The dissolved thrombin was then transferred to LoBind protein microtubes and stored in the freezer at −80 °C.

**Incubation cell.** An incubation chamber was designed to sandwich the gold SPE between two Perspex layers to reduce droplet leakage between electrodes. The top layer had a hole drilled precisely to expose the WE to the immobilization droplet, while covering the RE and CE. To ensure a secure and tight fit, neodymium magnets were used to hold the Perspex layers together. Schematics and images of the incubation chamber are provided in the SI, detailing the design and assembly process (Fig. S1).

## Methods

**Electrochemical characterization.** A compact potentiostat (PalmSens4) was used for electrochemical analysis of gold SPEs. Results were analyzed by an electrochemical analysis software (PStrace, PalmSens). All measurements were performed in a dark box to minimize light exposure. A Teflon cap was designed to slide the gold SPE inside the glass cell with two narrow holes for the $N_2$ gas inlet and outlet. EIS was performed to characterize charge transfer processes at the electrode interface by applying an alternating voltage of 5 mV and a biasing DC potential at the open circuit potential (OCP) *vs.* the Ag/AgCl reference electrode with a frequency range from 0.1 Hz to 100 kHz. Cyclic voltammetry (CV) was scanned twice in the measurement buffer solution to characterize the redox peaks within a potential window from −0.2 to 0.4 V at a scan rate of 50 mV $s^{-1}$ and a step of 5 mV. For the determination of electrochemically active surface area, gold SPEs were scanned three times using CV in 0.5 M $H_2SO_4$ from 0 to 1.4 V with a scan rate of 0.1 V $s^{-1}$, 5 mV per step. This step is known as electropolishing.

**Aptamer immobilization.** The 5 μM aptamer solution had a concentration of 40 μg $mL^{-1}$ and an $A_{260}/A_{280}$ ratio of 1.81 as analyzed by a microvolume spectrophotometer (NanoDrop, Thermo Fisher Scientific). The aptamer's aliquot was annealed in a dry bath heater at 90 °C for 5 minutes and then cooled slowly to reach room temperature. Then, 5 μL of the co-immobilization aliquot was drop-casted on the electrodes. The incubation chamber was put inside a humidity chamber and incubated at 25 °C for 16 h. Next, the electrodes were rinsed with incubation buffer and dipped in the same buffer for 10 minutes. Then, each electrode was rinsed with the measurement buffer and inserted into the electrochemical cell for electrochemical characterization.

**Protein incubation.** Thrombin's aliquot was taken out from the freezer (−80 °C) and thawed to room temperature. Gold SPEs were inserted into the incubation chamber. Then, 5 μL of the aliquot was drop-casted on the electrodes in the incubation chamber. The incubation chamber was put inside a humidity chamber and incubated at room temperature for 30 minutes. Next, the electrodes were dipped in the incubation buffer for 10 minutes and then rinsed with the measurement buffer and inserted into the electrochemical cell for electrochemical characterization.

**Plasma cleaning.** A plasma cleaner (PDC-002 Expanded plasma cleaner, Harrick Plasma), equipped with a vacuum pump, was used for surface cleaning of gold SPEs. This system has three power levels applied to an RF coil, including low (7 W), medium (11 W) and high (30 W). The gold SPEs were affixed to two slides of polystyrene films using adhesive tape to ensure stability during the cleaning process. To expose only the working electrode to plasma while covering the rest of the electrode, a hole with a diameter of 3 mm, matching the size of the working electrode, was drilled into the top polymeric film. The plasma cleaning was conducted at approximately 0.7 torr with a tolerance of ±0.05 torr.

**Surface chemistry.** An X-ray Photoelectron Spectroscopy (XPS) instrument (K-alpha$^+$, Thermo Fisher Scientific) with a monochromatic Al Kα X-ray source was used to characterize the surface chemistry of gold SPEs. Ten survey scans and five high-resolution scans of major elements (carbon, oxygen, nitrogen, and phosphorus) were taken on each sample for

comparison. Element peak areas were divided by element-specific sensitivity factors and converted to atomic percentage for each element. Results were analyzed by surface analysis software (Avantage Data System, Thermo Fisher Scientific).

**Surface wettability.** Water contact angle (WCA) measurements were performed on gold SPEs to evaluate the effect of plasma cleaning on surface wettability using a Theta tensiometer (Biolin Scientific). Results were averaged over 3 drops for each sample.

**Surface morphology.** Scanning electron microscopy (SEM) images were collected to analyze surface morphology and particle size on the gold SPE using an electron microscope (Scios 2, Oxford Ultim Max 170 EDS detector, Thermo Fisher Scientific) and were analyzed by microscopy analysis software (Aztec, Oxford Instruments).

## Results and discussion

### Mechanism of plasma cleaning

The commercial radio frequency (RF) discharge plasma cleaner consists of a coil wrapped around an insulating layer that houses a sealed chamber (schematic is depicted in Fig. 1A). An external RF power source energizes the cylindrical coil, creating a fluctuating magnetic field in its vicinity.[28] This magnetic field induces an alternating electric field that accelerates electrons in the working gas within the reaction chamber (digital image is shown in Fig. 1B). Once the kinetic energy of the residual free electrons exceeds the ionization threshold of the gas molecules and atoms, ionization occurs resulting in the formation of positively charged ions and more free electrons.[28] Low-pressure air plasma cleaning effectively removes organic contaminants from large-aperture optical components *in situ* within inertial confinement fusion facilities. During this cleaning process, reactive species are formed, including C–O, C=C, C=O, and O–H bonds, with C=O being the final product. The radicals O, $HO_2$, and $O_3$ are shown to be key components in breaking down contaminants.[29] First, the effect of air plasma cleaner on the electrochemical properties of the commercial gold SPEs were studied. As mentioned earlier in the experimental section, the gold SPEs were sandwiched between two slides of polystyrene films (Fig. 1C) only exposing the working electrode to the air plasma. The digital image of the gold SPE and its components (silver/silver chloride paste reference electrode, gold counter electrode and connecting wires) are provided in Fig. 1D. Used gold SPEs, containing immobilized DNA-based aptamer SAMs and thrombin, were exposed to the air plasma to regenerate the surface. The electrochemical and surface chemistry of the plasma-treated electrodes were studied next.

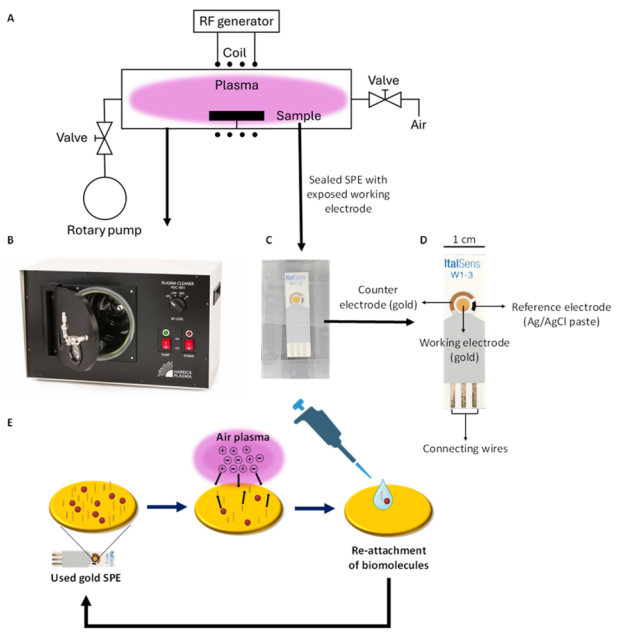


Fig. 1 (A) Schematic of an RF discharge plasma cleaner. (B) Digital images of the plasma cleaner (Harrick Plasma, PDC-002), (C) the gold SPE sample (Palmsens, Italsens gold SPE) sandwiched between two polystyrene films and (D) magnified digital image of the gold SPE showcasing its components. (E) Schematic of gold SPE regeneration cycle for biosensor fabrication and electrode reuse by air plasma cleaning.

### Influence of air plasma cleaning parameters on gold SPEs

The parameters of the plasma source, including power and treatment time, to regenerate gold SPEs were investigated. The "used gold SPEs" referred to those that were utilized for the fabrication of thrombin-binding aptasensors. They consisted of thiol-bonded, chemisorbed SAMs of the thrombin-binding aptamer, along with the bonded thrombin used for aptasensor fabrication and characterization. The used gold SPEs were exposed to an air plasma for different durations with two levels of power, and the results are shown in Fig. 2A. Pre-immobilized functional biomolecules partially blocked electron transfer processes on the electrode-solution interface. Therefore, the charge transfer resistance ($R_{ct}$) of the electrodes was measured using the faradaic EIS technique in the measurement buffer solution (containing ferro/ferricyanide redox couple) to evaluate the effectiveness of air plasma cleaning to remove the electron transfer barriers. Air plasma cleaning reduced the $R_{ct}$ of used electrodes that had been utilized to fabricate thrombin-binding aptasensors. By applying 10 minutes air plasma at high power (30 W, power density of ≈10 mW $cm^{-3}$) on the used electrodes, the barriers to charge transfer, including the SAMs of thiol-modified aptamers and the aptamer–thrombin complex, were removed. This removal resulted in a significant decrease in the $R_{ct}$ values from 8.3 kΩ to 0.9 kΩ which was similar to that of new electrodes (1.2 kΩ).

The resulting Nyquist plots and CV of electrodes with and without plasma modification are shown in Fig. 2B and C, respectively. The semi-circle in the Nyquist plot representing the $R_{ct}$ showed a significant reduction following plasma cleaning, since the surface was cleaned by removal of the immobilized biomolecules and excess binders. Though the new electrodes exhibited reversible redox peaks with distinct oxidation and reduction peaks (Fig. 2C), the plasma-cleaned electrode showed a smaller peak-to-peak separation ($\Delta E_{peak}$ ≈ 0.11 V) drawing closer to the ideal reversible nernstian behavior

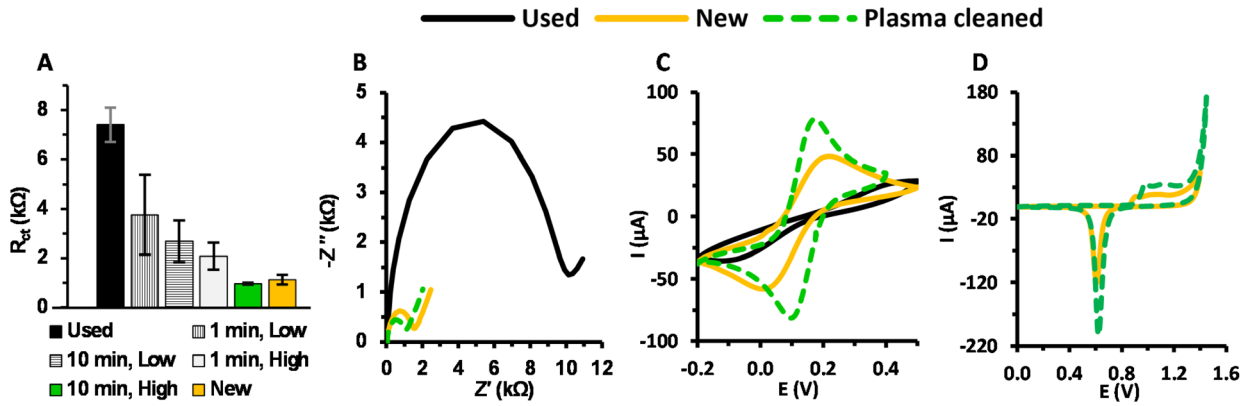


Fig. 2 (A) Effect of different plasma treatment time and power on $R_{ct}$ (obtained from circuit fitting of an equivalent Randles circuit) provided by faradaic EIS in the measurement buffer solution ($E_{ac} = 10$ mV $E_{dc} = E_{OCP}$, frequency range 100 kHz to 0.1 Hz). Error bars are included to represent the variability in the data collected from two different gold SPEs for each condition, with the measurements taken after a single cleaning of the sensors. (B) Nyquist plots ($E_{ac} = 10$ mV $E_{dc} = E_{OCP}$, frequency range 100 kHz to 0.1 Hz) and (C) CV of a used, plasma cleaned, and a new gold SPE in the measurement buffer solution *vs.* Ag/AgCl pseudo reference electrode (scan rate of 0.1 V $s^{-1}$). (D) CV of gold SPE in 0.5 M $H_2SO_4$ (electropolishing) of new and plasma cleaned gold SPEs *vs.* Ag/AgCl pseudo reference electrode (scan rate of 0.1 V $s^{-1}$).

associated with the transfer of a single electron from the $Fe(CN)_6^{4-/3-}$ redox probe. Meanwhile, the highest oxidation peak of $Fe(CN)_6^{4-}$ to $Fe(CN)_6^{3-}$ redox probe was observed on the plasma cleaned electrode (77.4 μA *vs.* new 44.5 μA). In contrast, the used electrode poorly represented a reversible redox reaction; its response resembled that of a pure resistor, with the current increasing almost linearly with voltage, in accordance with Ohm's law.

Pre-treatment of a gold electrode is commonly done by CV in 0.5 M $H_2SO_4$, providing gold atoms in a reduced state. This process is known as electropolishing and is shown in Fig. 2D. Several parameters were calculated from the cathodic peak of gold, including the electrodes' real surface area ($S_{true}$) and roughness factor ($r$). The integral from 0.5 V to 0.7 V of the cathodic (reduction) peak, which is the reduction of $Au^{3+}$ to Au, is used to calculate the total charge ($Q$).[30] The integral from a current–potential ($i$–$E$) curve is the power ($i \times E$), and was divided by the scan rate ($v$) to get the charge according to the eqn (1).

$$Q = \frac{\int_{V_1}^{V_2} I\,dv}{v} \quad (1)$$

The working electrode roughness factor ($r$) was estimated based on a well-developed protocol for calculating the electrode's true surface from the charge in the range of oxygen reductive desorption.[31] The true electrode surface ($S_{true}$) was the actual reactive area, while the geometrical surface ($S_{geom}$) is based on the electrode surface area ($\pi r^2$). The charge ($Q_{red}$) for oxygen electro-desorption was divided by 400 μC $cm^{-2}$, the charge needed to desorb an oxygen monolayer from 1 $cm^2$ (eqn (2)).[32] Roughness factor ($r$) was calculated based on the ratio of true electrode surface to its geometrical area (eqn (3)).[32]

$$S_{true} = \frac{Q_{red}\ (\mu C)}{400\ (\mu C\ cm^{-2})} \quad (2)$$

$$r = \frac{S_{true}}{S_{geom}} \quad (3)$$

The new electrodes provide an effective surface area of 0.21 $cm^2$ with a roughness factor of 2.97. These values are comparable to previously reported metrics for similar commercial gold SPEs, including Metrohm BT and AT gold SPEs with electroactive surface area of ≈0.26 $cm^2$ and 0.1 $cm^2$, respectively, with roughness factors ranging from 1.34 to 2.[22,33] While limited data are available on the roughness factor of gold SPEs, the values reported here offer a reference for future studies. Meanwhile, plasma cleaned electrodes exhibit higher effective surface area of 0.26 $cm^2$ with a rougher surface ($r = 3.64$). The increased surface roughness and electroactive area provide higher signal gain, underpinning high-performance biosensing applications.[14,34]

## Electrode characterization by electrochemical impedance spectroscopy (EIS)

In EIS characterization of an electrochemical sensor, the working electrode is perturbed by applying a small amplitude excitation alternating voltage ($V_0$) superimposed on a fixed voltage, commonly open circuit potential (OCP) or to the formal potential of the redox probe in the measuring solution.[35] The Randles circuit is the most frequently used model, as it effectively represents uncompensated resistance ($R_u$), charge transfer resistance ($R_{ct}$), Warburg impedance ($Z_W$), and double layer capacitance ($C_{dl}$). By fitting the impedance data to this equivalent circuit using appropriate modelling software, the values of each electrical component can be accurately calculated.

The capacitance ($C$) is calculated by eqn (4).[35]

$$C = \varepsilon\varepsilon_0\left(\frac{A}{d}\right) \quad (4)$$

where $\varepsilon$ is the dielectric constant of the medium at the electrode/electrolyte interface, $\varepsilon_0$ is the permittivity of free

space, $A$ is the electrode's surface area, and $d$ is the thickness of attached layers on the electrode's surface. In some cases, the capacitance element in the Randles circuit in electrochemical sensors is drifted from an ideal capacitance. In a non-ideal behavior of capacitance, the term constant phase element $Q_0$ is used. In a Randles circuit with semi-finite diffusion, the effective capacitance is given by eqn (5). In a Randles circuit with semi-finite diffusion, the effective capacitance is given by eqn (5).[36,37]

$$C = Q_0^{\frac{1}{n}}\left(\frac{1}{R_u} + \frac{1}{R_{ct}}\right)^{\frac{n-1}{n}} \quad (5)$$

$Q_0$ has the numerical value of the admittance $(1/|Z|)$ at $\omega = 1$ rad $s^{-1}$. $n$ is the exponent in the CPE impedance equation. In the case of an ideal capacitor, $n = 1$, and $C = Q_0$; However, the capacitance element in the Randles circuit in electrochemical sensors has typically drifted from an ideal capacitance. When $n < 1$, the CPE represents a non-ideal capacitive behavior, often due to surface roughness and varying thickness or composition of coatings.[35]

The gold SPEs were characterized using the EIS technique in a solution containing the redox couple, ferro/ferricyanide and TBS buffer (pH 7.4) to measure the equivalent electrical components. The EIS data presented here reveal relationships between surface modifications and their resulting electrochemical properties. The most significant trends emerge in the $R_{ct}$ and effective capacitance ($C$) parameters. As mentioned earlier, the decrease in $R_{ct}$ is related to the removal of excess organic binders and post-manufacturing contamination, with a parallel increase in capacitance (plasma cleaned 3.19 μF *vs.* control group without plasma cleaning 1.33 μF). This increase is explained by the decrease in dielectric thickness and an increase in electrochemical surface area, as capacitance follows an inverse relationship with layer thickness and a proportional relationship to surface area ($C \propto A/d$). The observation that the $R_{ct}$ remains relatively low following plasma surface cleaning suggests that the electron transfer process at the electrode interface is not significantly limited by heterogeneous electron transfer kinetics but instead, predominantly governed by mass transfer impedance. The electrochemical characteristics of a new (untreated), used, and plasma cleaned gold SPE showcasing the improved electrochemical performance and higher surface area *via* air plasma cleaning is shown in Table S1. The heterogenous electron transfer rate of plasma cleaned electrodes increased from $(5.48 \pm 0.08) \times 10^{-4}$ cm $s^{-1}$ to $(6.51 \pm 0.18) \times 10^{-4}$ cm $s^{-1}$. Moreover, we provided Table S2 as to compare the key differences in the treatment time, plasma power, sample size, pressure, and the main advantages/limitations of our work to the previous studies, providing a benchmark for future work. This plasma cleaning method can be used for pretreatment of unmodified gold SPEs to increase their heterogenous charge transfer rate and electrochemical active surface area.

### Mass transfer diffusion of redox active species

To better understand the diffusion process, we investigated how the scan rate affects the peak current in cyclic voltammetry experiments. We used the Randles–Sevcik equation to derive the diffusion coefficient. Additionally, we conducted parallel diffusion calculations from EIS by analyzing the Warburg impedance. The Warburg impedance, denoted as $Z_W$, characterizes the challenges associated with the mass transport of redox species to the electrode surface by considering a semi-infinite linear diffusion. $Z_W$ acts like a series circuit composed of a resistance ($R_w$) and a capacitance ($C_w$), both of which vary with frequency. Warburg coefficient $\sigma$ is defined by eqn (6).[35]

$$\sigma = \frac{2RT}{n^2F^2A\sqrt{2}\sqrt{D_0}C_0} \quad (6)$$

Plasma cleaning increases roughness and area, lowering charge transfer resistance, but the complex surface can hinder effective diffusion, resulting in a lower apparent $D_0$. Rewriting eqn (6) based on plotting the $i_p$ *vs.* $v$ provides the diffusion coefficient. Fig. S2 demonstrates the cyclic voltammograms of Randles–Sevcik experiments with plasma cleaned/electropolished gold SPE in ferric/ferrocyanide solution. The diffusion coefficient ($D_0$) of the redox couple is assumed to be equal for both the oxidized ($D_{ox}$) and reduced ($D_{red}$) forms. The other symbols retain their previously defined meanings, and their values are shown in Table S3. The $\sigma$ value was derived by plotting the imaginary impedance $-Z''$ *vs.* $\omega^{-1/2}$. The slope of this plot provided $\sigma$, which is shown in Table S4. An alternative method to derive $D_0$ is based on the Randles–Sevcik method. In processes involving electrochemically reversible electron transfer with freely diffusing redox species, the Randles–Sevcik equation (eqn (7)) illustrates how the peak current $i_p$ (A) correlates linearly with the square root of the scan rate $v$ (V $s^{-1}$).

$$i_p = 0.446nFAC_0\left(\frac{nFvD_0}{RT}\right)^{\frac{1}{2}} \quad (7)$$

In eqn (7), $n$ represents the number of electrons involved in the redox reaction, $A$ ($cm^2$) denotes the electrode's surface area (typically regarded as the geometric area), $D_0$ ($cm^2$ $s^{-1}$) indicates diffusion coefficient of the oxidized species, and $C_0$ (mol $cm^{-3}$) refers to the bulk concentration of the analyte. Diffusion coefficients were calculated using the Randles–Sevcik equation with parameters from Table S3.

Scan rate-dependent oxidation currents revealed linear correlations consistent with diffusion-controlled processes (Table S5). Both diffusion coefficients, calculated using the Randles–Sevcik equation from voltammetry tests and the EIS technique, showed a trend indicating that regenerated electrodes had lower diffusion coefficients, as presented in Table 1.

Table 1 Diffusion coefficient ($D_0$) of gold SPE with and without plasma cleaning derived from two electrochemical techniques based on CV and EIS

| Electrode | $D_0$ $cm^2$ $s^{-1}$ (CV) | $D_0$ $cm^2$ $s^{-1}$ (EIS) |
|---|---|---|
| Au/E-polished | $5.86 \times 10^{-6}$ | $6.84 \times 10^{-7}$ |
| Au/plasma-treated/E-polished | $5.01 \times 10^{-6}$ | $3.68 \times 10^{-7}$ |

Table 2 Water contact angle (WCA) and atomic percentage analysis results from XPS of three gold SPEs are reported based on the average value ± absolute error for three individually tested electrodes

| Gold SPE | WCA° | Au% | C% | O% | N% |
|---|---|---|---|---|---|
| New | 101 ± 3.0 | 20.1 ± 0.19 | 53.8 ± 1.2 | 20.5 ± 0.21 | 5.6 ± 0.030 |
| Used | 76 ± 7.6 | 13.9 ± 0.13 | 54.9 ± 0.48 | 20.7 ± 0.040 | 10.5 ± 0.30 |
| Plasma cleaned | 33 ± 2.3 | 22.5 ± 0.23 | 43.6 ± 0.18 | 25.3 ± 0.16 | 8.5 ± 0.040 |

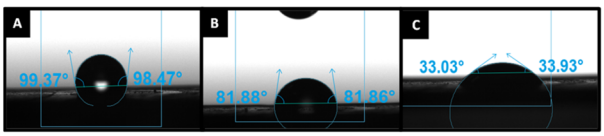


Fig. 3 Water contact angle of (A) new, (B) used and (C) 10 minutes air plasma cleaned gold SPE.

The reasoning behind this phenomenon may be complex, but one study suggests that increased roughness can lead to a more tortuous diffusion path, which could potentially slow down diffusion and subsequently affect the measured diffusion coefficient.[38]

### Surface chemistry analysis by XPS and water contact angle

XPS analysis was conducted to investigate changes in the surface chemistry of the electrodes after plasma cleaning. Table 2 summarizes the elemental surface composition of the electrodes subjected to different treatments. Used electrodes showed the lowest Au% (≈13.9%) and the highest C% (≈54.9%), as a result of attached biomolecules and residual binder. New electrodes had a higher Au% (≈20.1%) with a slight reduction in C% (≈53.8%). Plasma cleaning enhanced Au% (≈22.5%) and significantly reduced C% (≈43.6%). However, air plasma cleaning increased O% (≈25.3%), which could be due to the binder oxidation. Water Contact Angle (WCA) measurements indicated that new gold SPEs (Fig. 3A) show hydrophobic surfaces (101°), stemming from pasting binder and other post-manufacturing sources of contamination. This WCA decreased to approximately 76° (Fig. 3B) after immobilizing water-soluble molecules like aptamers and proteins. Plasma-treated electrodes showed a significant decrease of WCA to 33° (Fig. 3C) by removing the excess binders and oxidation with more oxygen-containing groups. The Au 4f core-level photoelectron spectra (Fig. 4A) exhibited a doublet including Au $4f_{7/2}$ and Au $4f_{5/2}$ peaks at 84.0 eV and 87.7 eV respectively. The observed spin–orbit splitting ($\Delta E = 3.7$ eV) is consistent with pure metallic gold ($Au^0$), in agreement with the ref. 39. Although previous studies showed that $O_2$ plasma results in gold oxidation as confirmed by 1 eV shift in the Au $4f_{7/2}$ band, we did not observe such oxidation and shift in gold photoelectron spectra.[40–42] Moreover, new electrodes exhibited significant surface carbon C 1s peaks as a result of excess pasting binders and post-manufacturing contamination.[22] After plasma treatment, the intensity of the C 1s peak decreases due to the removal of excess binders and tethered biomolecules (Fig. 4B). DNA-based aptamers and proteins contain amine-based functional groups, which resulted in a significant nitrogen peak from pre-attached biomolecules. The removal efficiency of these biomolecules is evaluated by the reduction of the N 1s to the noise level, after plasma treatment (Fig. 4C). The reduction in the peak intensity for both carbon and nitrogen after air plasma treatment indicates the removal of excess organic binders and tethered biomolecules with slight oxidation as observed in the increased O 1s peak (Fig. 4D). A table comparing our obtained XPS data for the peak binding energies of the four analyzed elements with previously published binding energy data is provided in Table S6. In summary, our results of peak binding energy and spin–orbit coupling energy are comparable with the literature and provide a benchmark of gold SPE XPS characterization for future studies.

### Nyquist and Bode plot analysis of gold SPE

Having confirmed the effective removal of organic contaminants and biomolecules by plasma treatment, the electrodes were subsequently characterized in the measurement buffer using the EIS technique. It was notable to witness, by

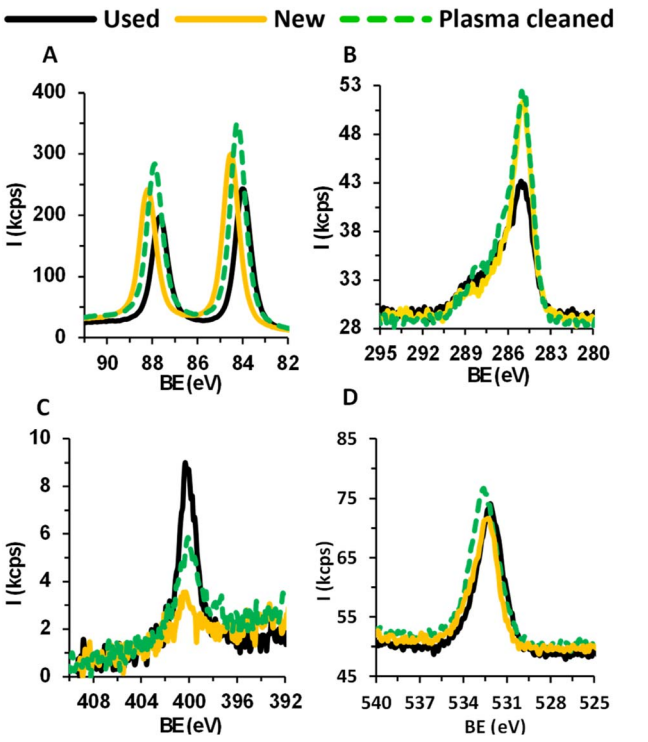


Fig. 4 Overlaid photoelectron spectra of (A) Au 4f, (B) C 1s (C) N 1s, and (D) O 1s.

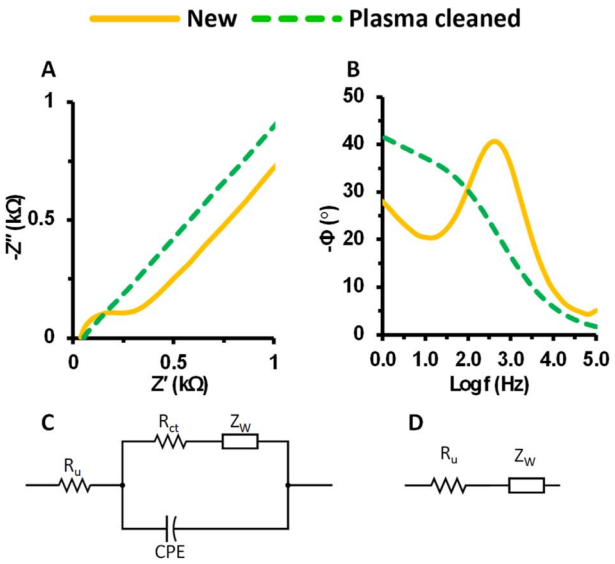


Fig. 5 Nyquist plot (A) and Bode plot (B) of a new and plasma regenerated gold SPEs after electropolishing in the measurement buffer solution ($E_{ac} = 10$ mV $E_{dc} = E_{OCP}$, frequency range 100 kHz to 0.1 Hz). Equivalent circuit of a new electrode (C) and plasma regenerated electrode after electropolishing (D).

electropolishing the plasma-treated electrodes in sulfuric acid, that the semi-circle in the Nyquist plot of the regenerated gold SPE diminished. In a Nyquist plot, the imaginary component of impedance ($-Z''$) is plotted against the real component of impedance ($Z'$) over a wide range of excitation frequencies (Fig. 5A). In the case of electropolished and air plasma regenerated electrodes, the electron transfer was remarkably kinetically facile. In reversible electrochemical systems with fast kinetics, $R_{ct}$ becomes negligible compared to the $R_u$, and the $Z_W$ dominates across the entire frequency range.[35] In such kinetically facile systems, the current is primarily governed by mass transfer, leading to a poorly defined semicircular region. The distinction between the kinetic and mass transfer regions depends on the relative magnitudes of $R_{ct}$ and $Z_W$. Thus, in electropolished plasma cleaned electrodes, the current is only limited by mass transfer of redox couple,[35] and the semicircular region was not well-defined. Hence, the impedance of the regenerated electrode was mainly governed by the Warburg impedance, which was observed as a straight line at 45° on the abscissa.

Moreover, the peak phase ($\varphi$) in the Bode plot of the plasma-regenerated electrode was diminished since the impedance was mainly controlled by mass transfer (Fig. 5B). The Bode plot further clarified the frequency-dependent behavior of the regenerated electrodes. The $-\varphi$ *vs.* frequency curve showed a diminished phase shift, supporting the hypothesis of kinetically facile electron transfer. The logarithmic scaling of both axes in the Bode plot provides a clearer visualization of these trends to emphasize the efficiency of the plasma-treated surfaces in minimizing interfacial resistance and capacitive effects. In contrast, for new electrodes, the phase shift increased until it reached a maximum, where both resistive and capacitive elements of the Randles circuit affected the system. To analyze these results, an equivalent electrical circuit based on a modified Randles circuit that modeled the electrochemical sensor was defined (Fig. 5C). Consequently, the equivalent Randles circuit of the electrodes was simplified to a circuit consisting of uncompensated resistance ($R_u$) and Warburg impedance ($Z_W$) when they were treated with air plasma and electropolishing as shown in Fig. 5D. In summary, electropolishing the plasma-recycled electrodes resulted in negligible $R_{ct}$ compared to $R_u$; therefore a very fast charge transfer kinetics. This shift simplified the impedance response, as the interface was dominated by mass transfer processes rather than electron transfer rates. The diminished influence of the $C_{dl}$ and $R_{ct}$ eliminates the semicircular feature in Nyquist plots, leaving the $Z_W$ as the primary determinant of the system's behavior. Consequently, the equivalent circuit reduced to a simple combination of $R_u$ and $Z_W$, reflecting a kinetically facile and mass-transfer-limited system.

## Aptasensor performance of regenerated gold SPE

After the used gold SPEs were regenerated using plasma treatment, their potential for reuse as aptasensors was evaluated. Aptamer loading efficiency and thrombin binding (aptasensor performance) were assessed by fabricating the aptasensor on the gold SPEs with three modifications, including: (1) new, (2) plasma-regenerated, and (3) electropolished plasma-regenerated gold SPEs. The Nyquist plots obtained from the EIS analysis of the sensors were modelled by the Randles circuit to calculate the $R_{ct}$ of the redox couple. $R_{ct}$ increased upon aptamer immobilization since the aptamer's monolayer impeded the facile electron transfer from the charged redox couple to/from the electrode.[43] This was related to the electrostatic repulsion between the negatively charged phosphate backbone of aptamers and redox couple, along with the densely packed SAMs that create a barrier to diffusion from the bulk solution to the electrode surface.[43,44] Furthermore, $R_{ct}$ increased significantly after thrombin binding since the bulky protein layer disrupted electron transfer between the electrode and the redox couple.[45] It was observed that the aptamer loading efficiency of the regenerated gold SPEs without electropolishing was lower than that of new gold SPEs as shown in Fig. 6A. Aptamer immobilization led to $3.4 \pm 0.4$ kΩ for the new gold SPE *versus* $1.0 \pm 0.3$ kΩ for the plasma-regenerated gold SPEs, with corresponding thrombin binding $R_{ct}$ responses of $7.3 \pm 0.5$ kΩ and $4.1 \pm 0.9$ kΩ, respectively. Consequently, regenerated SPEs were electropolished by CV in $H_2SO_4$ to reduce the gold atoms and to improve thiol–gold SAM formation.[22,46,47] After electropolishing, aptamer immobilization and aptasensor performance improved substantially, with the electropolished plasma-regenerated SPEs increasing the $R_{ct}$ to $6.8 \pm 1.2$ kΩ by aptamer immobilization and a significant increase in $R_{ct}$ by thrombin binding to $37 \pm 4$ kΩ (Fig. 6B). The sensor's signal which is the relative change in $R_{ct}$ for plasma modified electrodes after thrombin incubation is higher than unmodified electrodes, therefore, the plasma modified sensors are more sensitive to detect thrombin. The enhancement in aptamer loading and thrombin binding was likely due to the strong regeneration and cleaning efficiency of air plasma, which effectively removes

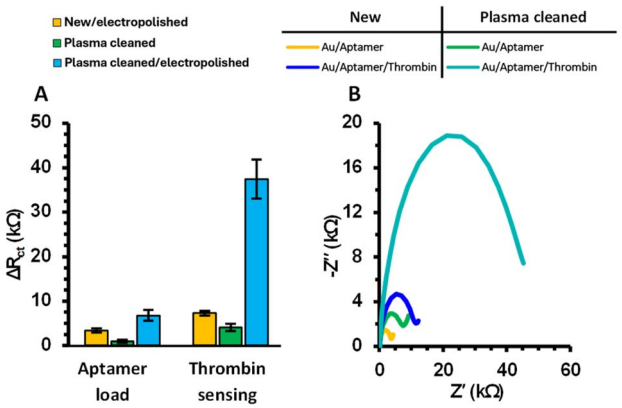


Fig. 6 (A) Aptamer load and aptasensor performance (thrombin sensing) of gold SPEs undergoing different treatments based on the change in charge transfer resistance ($\Delta R_{ct}$) for three individually tested electrode in each category. (B) Nyquist plots of gold SPE-based aptasensor (5 μM aptamer, 50 nM thrombin). All measurements were carried out in the measurement buffer solution.

biomolecules and post-manufacturing surface contamination. The enhanced thrombin sensing performance was evident in the Nyquist plot of the electropolished plasma-regenerated electrodes, which showed a significantly larger semicircle compared to the new electrodes. In previous studies, similar improvements in electrochemical properties were observed in screen-printed carbon electrodes, where low-level oxygen plasma effectively removed the non-conductive binder covering the graphite grains on the electrode's surface.[48,49]

### Effect of repeated cycles of plasma cleaning on gold SPE: removal of mercaptohexanol SAMs

Recycling the electrodes, even once, could reduce the environmental impact and cost of biosensor fabrication. We investigated whether the electrode remains integrated and functional after three cycles of air plasma cleaning. The impact of successive plasma cleaning cycles on the electrochemical properties of electrodes was investigated, with a particular focus on $R_{ct}$ and immobilization efficiency.

The process involved exposing the electrode to 25 mM mercaptohexanol (MCH), followed by air plasma cleaning and repeated E-polishing. We adapted the methodology from Raiber *et al.*, where the removal of hexadecanethiolate by $H_2$ plasma from a gold electrode was evaluated by Ellipsometry.[21] In our method, we observed that the new electrodes showed a $R_{ct}$ response of 0.37 ± 0.03 kΩ and, after MCH backfilling $R_{ct}$ increased to 1.2 ± 0.7 kΩ. The high standard deviation observed in the $R_{ct}$ following MCH immobilization, as reported for three electrodes, might be attributed to the fact that not all electrodes exhibit similar electrochemical behavior. This variability could stem from excess binder in the screen-printing process and contamination that occurred during manufacturing.[50] Additionally, the SAM formation of MCH was performed for only 1 hour in a humidity chamber. Although it has been shown that SAMs can form almost immediately upon incubation, they may take over 24 hours to reorganize, leading to some variability in results.[51] The first plasma cycle reduced the $R_{ct}$ to near-zero while the first plasma cycle followed by MCH increased the $R_{ct}$ to 1.4 ± 0.3 kΩ. The second plasma cycle again showed near-zero $R_{ct}$ and the second plasma cycle with MCH incubation increased the $R_{ct}$ to 1.0 ± 0.1 kΩ. The same pattern was observed after the third plasma cycle with a near-zero $R_{ct}$ of the plasma-cleaned electrodes (Fig. 7A). Improvements in the reproducibility of the immobilization process were observed following each cycle, as indicated by a decrease in the relative standard deviation (RSD) from 37% to 12%. To further assess the structural and compositional integrity of the printed gold microparticles following plasma treatment, SEM imaging was conducted, which revealed no significant changes in the morphology or surface structure of the gold particles (Fig. 7B–E). The microparticles retained their original structure, and no signs of surface degradation or elemental contamination were detected. In summary, we have shown that the gold SPEs can be recycled at least three times. In each cycle of cleaning, we observed a similar electrochemical behavior of plasma cleaned electrode *i.e.* near zero charge transfer resistance. Meanwhile, the peak potentials from cyclic voltammograms of a gold SPE in TBS 1× and ferro/ferricyanide 2 mM after three cycles of plasma cleaning overlapped, which means that the reference electrode is still functional and shows similar peak potential values

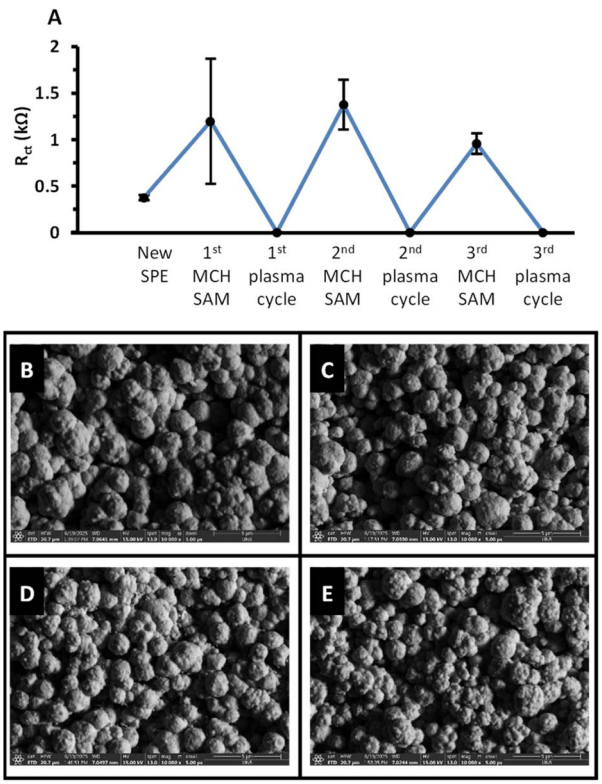


Fig. 7 Repeated cycles of plasma cleaning on gold SPE. (A) $R_{ct}$ measurements after repeated formation and removal of MCH SAM by air plasma in the measurement buffer solution. Error bars are based on three individually tested SPEs for each condition. SEM images of the gold electrode (B) without, (C) 1 cycle, (D) 2 cycles, and (E) 3 cycles of air plasma cleaning reveals no morphological/structural changes in the gold microparticles.

(Fig. S3). We did not observe any significant changes in the electrode morphology (such as electrode etching or pit holes) as shown in the SEM analysis. We must highlight the fact that the DNA-based aptamers and thrombin that were immobilized on the electrode, *i.e.*, the used electrodes, have a size of less than 3–5 nm; therefore, it would not be possible with the SEM magnification to observe such nanoscale biological compounds. The purpose of conducting SEM analysis was to observe bulk changes in the μm sizes and to determine if there is any significant etching (*i.e.* pit holes, detachment of gold particles from the binder). In our study, we lack the ultrasensitive magnification techniques to provide high-resolution images for analyzing attached biomolecules. Instead, we opted for XPS analysis that showed a decay in surface C% and N% and an increase in Au% after plasma cleaning, justifying the removal of biomolecules and excess pasting binders.

## Conclusions

Gold SPEs were regenerated by air plasma cleaning to remove surface-attached aptamer and thrombin. XPS and WCA measurement results showed that air plasma cleaning creates a hydrophilic surface with relatively low surface carbon content. Electropolishing plasma-regenerated gold electrodes resulted in a near-zero charge transfer resistance in ferro/ferricyanide solution. Meanwhile, electropolished plasma-regenerated electrodes exhibited improved aptasensor performance compared to new electrodes as a result of effective contaminant removal and increased electroactive surface area. In summary, air plasma cleaning enhances electrode performance through efficient removal of surface attached SAMs and excess binders, as evidenced by significant decrease in surface C% and N% and near-zero charge transfer resistance. Meanwhile, the developed air plasma cleaning technique contributes to sustainable biosensor development by recycling used SPEs. Future research should validate plasma regeneration and sensing performance across a wider range of electrode materials, such as alternative gold electrodes, carbon, and indium tin oxide. Moreover, it is essential to evaluate the immobilization and activity retention of other recognition elements and enzymes on plasma-regenerated electrodes for broader biosensing applications.

## Author contributions

All authors contributed to the preparation of this manuscript. Specific contributions are as follows: S. A. conceived of the original idea. S. A. planned the experiments. S. A., C. T., analyzed the data. S. A. conducted the experiments and wrote the manuscript. S. A., C. T., S. F., M. B., and A. I. edited the manuscript. S. A., A. I., and M. B. supervised and acquired funding for the project. All authors discussed the results and contributed to the final manuscript.

## Conflicts of interest

The authors declare no conflict of interest.

## Data availability

The data supporting this article is available at UNB Libraries DATAVERSE Research Data Repository: https://doi.org/10.25545/DGGWZZ,

Supplementary information (SI) is available. See DOI: https://doi.org/10.1039/d6su00113k.

## Acknowledgements

This work was carried out with financial support of the New Brunswick Innovation Foundation NBIF (Project No. EP-0000000155) & New Brunswick Health Research Fund NBHRF (Project No. 0000000045) and MITACS Globalink Research Award Application Ref. IT36728. We thank Professor Vicki Meli (Mount Allison University) for access to plasma equipment, Steven Cogswell (UNB) for SEM analysis, Dr Kostadinos Tsoutas (University of Sydney) for his valuable advice and Chun Keat Khor (UNB) for assisting with plasma cleaning experiments. Funding from an Australian Research Council Laureate Fellowship (FL190100216) is gratefully acknowledged. We acknowledge funding from Australian Research Council (IM250100134).

## References

1 U. Chadha, P. Bhardwaj, R. Agarwal, P. Rawat, R. Agarwal, I. Gupta, M. Panjwani, S. Singh, C. Ahuja, S. K. Selvaraj, M. Banavoth, P. Sonar, B. Badoni and A. Chakravorty, *J. Ind. Eng. Chem.*, 2022, **109**, 21–51.
2 G. Paimard, E. Ghasali and M. Baeza, *Chemosensors*, 2023, **11**, 113.
3 C. Moonla, R. Del Caño, K. Sakdaphetsiri, T. Saha, E. De la Paz, A. Düsterloh and J. Wang, *Biosens. Bioelectron.*, 2023, **220**, 114891.
4 A. García-Miranda Ferrari, S. J. Rowley-Neale and C. E. Banks, *Talanta Open*, 2021, **3**, 100032.
5 *Global Screen-printed Electrodes Market 2024–2033*, https://www.custommarketinsights.com/report/screen-printed-electrodes-market/.
6 A. Villalonga, A. M. Pérez-Calabuig and R. Villalonga, *Anal. Bioanal. Chem.*, 2020, **412**, 55–72.
7 S. Singh, J. Wang and S. Cinti, *ECS Sens. Plus*, 2022, **1**, 023401.
8 S. Hassani, M. R. Akmal, A. Salek-Maghsoudi, S. Rahmani, M. R. Ganjali, P. Norouzi and M. Abdollahi, *Biosens. Bioelectron.*, 2018, **120**, 122–128.
9 J. Lee, H. N. Suh, H.-b. Park, H. J. Kim and S. Kim, *ACS Omega*, 2025, **10**, 49260–49271.
10 A. Mahmud, D. Chang, J. Das, S. Gomis, F. Foroutan, J. B. Chen, L. Pandey, C. D. Flynn, H. Yousefi, A. Geraili, H. J. Ross, E. H. Sargent and S. O. Kelley, *Angew. Chem., Int. Ed.*, 2023, **62**, e202213567.
11 Y. Yang, X. Gao, B. Widdicombe, X. Zhang, J. L. Zielinski, T. Cheng, A. Gunatilaka, K. K. Leung, K. W. Plaxco, R. Rajasekharan Unnithan and A. G. Stewart, *ACS Nano*, 2024, **18**, 26127–26139.

12 S. W. Abeykoon and R. J. White, *Anal. Chem.*, 2024, **96**, 6958–6967.
13 V. Vogiazi, A. De La Cruz, W. R. Heineman, R. J. White and D. D. Dionysiou, *Anal. Chem.*, 2021, **93**, 812–819.
14 Z. Watkins, A. Karajic, T. Young, R. White and J. Heikenfeld, *ACS Sens.*, 2023, **8**, 1119–1131.
15 *Gold Facts*, https://natural-resources.canada.ca/minerals-mining/mining-data-statistics-analysis/minerals-metals-facts/gold-facts.
16 *Reducing Mercury Pollution from Artisanal and Small-Scale Gold Mining*, https://www.epa.gov/international-cooperation/reducing-mercury-pollution-artisanal-and-small-scale-gold-mining.
17 M. Di-Oliveira, R. G. Rocha, M. C. Marra, T. C. Oliveira, M. Vojs, M. Marton, R. D. Crapnell, C. E. Banks, E. M. Richter and R. A. A. Muñoz, *Electrochim. Acta*, 2025, **537**, 146851.
18 F. Ghamouss, E. Luais, C. Thobie-Gautier, P. Y. Tessier and M. Boujtita, *Electrochim. Acta*, 2009, **54**, 3026–3032.
19 J. Sun, Y. Yu, J. Tang, Y. Zeng and J. Chen, *IEEE Access*, 2025, **13**, 37221–37242.
20 T. Sun, P.-Y. Blanchard and M. V. Mirkin, *Anal. Chem.*, 2015, **87**, 4092–4095.
21 K. Raiber, A. Terfort, C. Benndorf, N. Krings and H. H. Strehblow, *Surf. Sci.*, 2005, **595**, 56–63.
22 A. Makaraviciute, X. Xu, L. Nyholm and Z. Zhang, *ACS Appl. Mater. Interfaces*, 2017, **9**, 26610–26621.
23 M. Di-Oliveira, M. C. Marra, R. G. Rocha, T. R. Terra, R. A. A. Muñoz and E. M. Richter, *Anal. Chem.*, 2026, **98**, 1915–1927.
24 M. C. Marra, M. Di-Oliveira, R. G. Rocha, T. R. Terra, R. D. Crapnell, C. E. Banks, E. M. Richter and R. A. A. Muñoz, *Microchim. Acta*, 2026, **193**, 199.
25 J. C. Love, L. A. Estroff, J. K. Kriebel, R. G. Nuzzo and G. M. Whitesides, *Chem. Rev.*, 2005, **105**, 1103–1170.
26 D. M. Tasset, M. F. Kubik and W. Steiner, *J. Mol. Biol.*, 1997, **272**, 688–698.
27 *Thrombin from Human Plasma_Product Information*, https://www.sigmaaldrich.com/deepweb/assets/sigmaaldrich/product/documents/599/516/t6884pis.pdf.
28 T. C. Isabell, P. E. Fischione, C. O'Keefe, M. U. Guruz and V. P. Dravid, *Microsc. Microanal.*, 1999, **5**, 126–135.
29 Y. Li, Q. Bai, Y. Guan, H. Liu, P. Zhang, B. Batelibieke, R. Shen, L. Lu, X. Yuan, X. Miao, W. Han and C. Yao, *Plasma Sci. Technol.*, 2022, **24**, 064012.
30 K. Ogura, S. Haruyama and K. Nagasaki, *J. Electrochem. Soc.*, 1971, **118**, 531.
31 V. M. Andoralov, M. R. Tarasevich and O. V. Tripachev, *Russ. J. Electrochem.*, 2011, **47**, 1327–1336.
32 S. N. Ovchinnikova and A. Z. Medvedev, *Russ. J. Electrochem.*, 2015, **51**, 287–293.
33 M. Zamani, V. Yang, L. Maziashvili, G. Fan, C. M. Klapperich and A. L. Furst, *ACS Meas. Sci. Au*, 2022, **2**, 91–95.
34 N. Arroyo-Curras, K. Scida, K. L. Ploense, T. E. Kippin and K. W. Plaxco, *Anal. Chem.*, 2017, **89**, 12185–12191.
35 A. C. Lazanas and M. I. Prodromidis, *ACS Meas. Sci. Au*, 2023, **3**, 162–193.
36 B.-Y. Chang, *J. Electrochem. Sci. Technol.*, 2020, **11**, 318–321.
37 B.-Y. Chang, *J. Electrochem. Sci. Technol.*, 2022, **13**, 479–485.
38 T. Tichter, A. Tichter, D. Andrae and C. Roth, *Electrochim. Acta*, 2024, **508**, 145175.
39 Y. Xue, X. Li, H. Li and W. Zhang, *Nat. Commun.*, 2014, **5**, 4348.
40 H. T. N. Le, L. M. T. Phan and S. Cho, *Materials*, 2022, **15**, 2218.
41 F. Vitale, I. Fratoddi, C. Battocchio, E. Piscopiello, L. Tapfer, M. V. Russo, G. Polzonetti and C. Giannini, *Nanoscale Res. Lett.*, 2011, **6**, 103.
42 K. Juodkazis, J. Juodkazyte, V. Jasulaitiene, A. Lukinskas and B. Sebeka, *Electrochem. Commun.*, 2000, **2**, 503–507.
43 A. E. Radi, J. L. A. Sánchez, E. Baldrich and C. K. O'Sullivan, *Anal. Chem.*, 2005, **77**, 6320–6323.
44 H. Cai, T. M.-H. Lee and I. M. Hsing, *Sens. Actuators, B*, 2006, **114**, 433–437.
45 A. E. Radi, J. L. Acero Sanchez, E. Baldrich and C. K. O'Sullivan, *Anal. Chem.*, 2005, **77**, 6320–6323.
46 Z. Li, L. Zhang, S. Zeng, M. Zhang, E. Du and B. Li, *J. Electroanal. Chem.*, 2014, **722–723**, 131–140.
47 G. Feng, T. Niu, X. You, Z. Wan, Q. Kong and S. Bi, *Analyst*, 2011, **136**, 5058–5063.
48 X. F. Yuan, L. L. Ma, J. Zhang and Y. Zheng, *Appl. Surf. Sci.*, 2021, **544**, 148760.
49 K. Tamargo-Martínez, S. Villar-Rodil, A. Martínez-Alonso and J. M. D. Tascón, *Appl. Surf. Sci.*, 2022, **575**, 151675.
50 K. Barman, S. Luhar, R. Rane, D. N. Srivastava, S. K. Nema and S. Bhattacharjee, *Plasma Processes Polym.*, 2023, **20**, 2200161.
51 R. Voicu, T. H. Ellis, H. Ju and D. Leech, *Langmuir*, 1999, **15**, 8170–8177.